Heliyon 9 (2023) e20936

Contents lists available at ScienceDirect

Heliyon

journal homepage: www.cell.com/heliyon

Structural and vibrational characterization of di-hydrated hydrochloride tacrine combining DFT with SQMFF approach

Tom Sundius [a], Silvia Antonia Brandán [b,*]

[a] Department of Physics, University of Helsinki, Finland
[b] Cátedra de Química General, Instituto de Química Inorgánica, Facultad de Bioquímica. Química y Farmacia, Universidad Nacional de Tucumán, Ayacucho 471, Tucumán, 4000, San Miguel de Tucumán, Argentina

ARTICLE INFO

Keywords:
Hydrochloride tacrine
Di-hydrated structure
Scaled force constants
Vibrational study
Hybrid calculations

ABSTRACT

This research is a continuation of previously reported article on anhydrous freebase, cationic and hydrochloride tacrine. Here, structures and properties of di-hydrated species of cholinesterase inhibitor tacrine have been studied in gas phase and aqueous solution by using B3LYP/6-311G* and wB97XD/6-311G* levels of theory. Both methods show strong changes in the positions of two water molecules and similar solvation energies (−192.52 kJ/mol with the B3LYP method and −191.95 kJ/mol with the other one). The B3LYP method predicts low gap values for the anhydrous (2.4572 eV) and di-hydrated (3.2708 eV) species of tacrine in gas phase than the wB97XD/6-311G* method (7.2300 eV). Hence, higher reactivities are expected for the di-hydrated species in both media. Atoms in molecules (AIM) calculations support the lower stability of di-hydrated species in solution in agreement with its higher reactivity in this medium. Complete assignments of 104 vibration modes expected for di-hydrated hydrochloride by using the scaled mechanical force field (SQMFF) methodology have been reported. Both methods predict different assignments and scaled force constants presenting higher values those calculated with the wB97XD/6-311G* method. The predicted IR, Raman and ^{1}H NMR spectra with both methods show good correlations with the corresponding experimental ones, however, better concordances between the ^{13}C NMR and UV spectra are observed with the wB97XD/6-311G* method.

1. Introduction

Recently, vibrational assignments and structural properties of anhydrous species of two cationic and three hydrochloride forms of cholinesterase inhibitor tacrine together with the freebase were studied combining hybrid B3LYP calculations with the scaled harmonic force fields [1]. The aim of that study was to elucidate the different cationic and hydrochloride structures of tacrine and, more specifically, to understand why the Cl atom of hydrochloride tacrine is experimentally linked to an H atom of NH_2 group instead H of NH group. Fig. 1 shows clearly that the positive charge of cationic species is located on the N atom of NH group while the Cl atom of hydrochloride form bonded to one H of NH_2 group. The explanation of that behaviour is related to the two water molecules bonded to hydrochloride species, one to H atom of NH group and the other one to Cl, which stabilize the structure of this form of tacrine as a di-hydrated species, as was experimentally observed (see Fig. 1) [2].

Thus, theoretical structures and structural, topological and vibrational properties of anhydrous species of tacrine were published

* Corresponding author.
E-mail address: silvia.brandan@fbqf.unt.edu.ar (S.A. Brandán).

https://doi.org/10.1016/j.heliyon.2023.e20936
Received 11 July 2023; Received in revised form 25 September 2023; Accepted 11 October 2023
Available online 12 October 2023

[1] and, due to the extension of that work was not possible to study the structures and properties of the di-hydrated species with the rigor and depth that are necessary to perform the complete vibrational assignments of this species of tacrine. As a continuation of that study and taking into account the importance of tacrine as a cholinesterase inhibitor used for treatment of Alzheimer's disease [3–6], the structures and properties of di-hydrated species of tacrine in gas phase and aqueous solution are here studied. Therefore, the theoretical initial structure of di-hydrated species of hydrochloride tacrine was taken from that experimental orthorhombic pseudo polymorph determined by X-ray diffraction [2]. Then, the structure of di-hydrated species was optimized in gas phase and aqueous solution by using B3LYP and wB97XD calculations. At that time, the vibrational spectra were completely assigned and compared with the previously reported for anhydrous hydrochloride tacrine [1,7,8]. Here, we consider the effects of dispersion in the di-hydrated species using the wB97XD method due to the presence of intra-molecular interactions generated by the two water molecules. This way, knowing that the method produces less stable structures with lower energy values (less negative values), as was reported for anhydrous tacrine and other species, comparisons of properties with those two B3LYP and wB97XD methods were performed [1,9,10]. To achieve those purposes, the experimental structure di-hydrated of hydrochloride tacrine was used as initial and, then, the optimizations were performed using the B3LYP method with the 6–311++G**, 6-311G* and 6-31G* basis sets [7,8]. After that, the complete vibrational assignments using the normal internal coordinates, transferable scaling factors and the harmonic force fields obtained with the SQMFF procedure and the Molvib program were accomplished [11–13]. Here, assignments of stretching, deformation and librations (wagging, rocking and twisting) modes of two water molecules have been performed and compared with those reported for the anhydrous species. When the di-hydrated species of tacrine is compared with the corresponding to trehalose very good concordances in the assignments and scaled force constants are observed [14].

2. Material and methods

The theoretical initial structure of di-hydrated hydrochloride tacrine was the experimental CIF file determined by Moris et al. by X-ray diffraction [2]. First, the B3LYP/6-31G* method was used to optimize the structures in gas phase and aqueous solution and, then, by using the other 6-311G* and 6–311++G** basis sets. Surprisingly, the calculations with the B3LYP/6–311++G** level of theory produces error in the internal coordinates system because the introduction of diffusion functions in the used basis set resulted unsatisfactory for the reproduction of the experimental wavenumbers. Thus, B3LYP/6-311G* calculations was employed, as in anhydrous tacrine [1]. Then, wB97XD/6-311G* calculations were also performed for the di-hydrated species in both media. For all calculations in both media the set of Gaussian 16 programs was used [15]. In solution, the polarizable continuum model (PCM) and universal solvation method (SMD) were employed [16–18]. The volume variations were computed by using the Moldraw program [19]. As in anhydrous tacrine, atomic charges, bond orders, stabilization energies and topological properties were computed with the natural bond orbital and atoms in molecules programs [20–22] while the Merz-Kollman charges and the *GaussView* program were used to calculate molecular electrostatic potentials (MEP) and the mapped MEP surfaces [23,24]. Frontier orbitals and chemical potential, electronegativity, global hardness, global softness and global electrophilicity index descriptors were used to predict reactivity and behaviour of di-hydrated species [25–28]. The harmonic force fields were computed with the SQMFF methodology and the Molvib program considering normal internal coordinates, transferable scaling factors and potential energy distribution (PED) contributions ≥10 % [11–13]. Hence, all bands observed in the experimental vibrational spectra of di-hydrated tacrine have been assigned. Predicted Raman spectra in activities are converted to intensities using know equations [29,30]. The GIAO method was employed to predict ^{1}H and ^{13}C NMR spectra while the electronic spectrum in aqueous solution was predicted by using the Gaussian 16 program [15]. Good correlations between the experimental and predicted NMR spectra have been obtained although the predicted electronic spectra by using the B3LYP/6-311G* method is different from that obtained with the wB97XD/6-311G* level of theory [29].

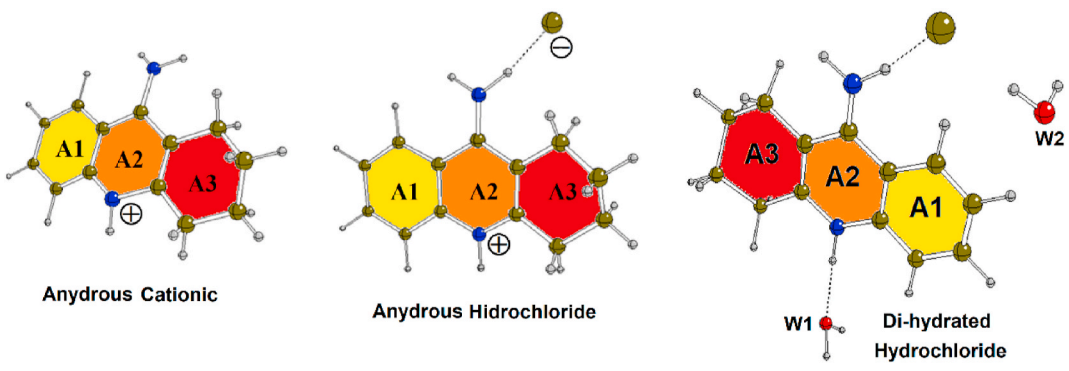

Fig. 1. Structures of anhydrous cationic and hydrochloride, and di-hydrated hydrochloride species of tacrine. Intramolecular H-bonds are represented with dashed lines while the water molecules as W1 and W2.

3. Results and discussion

3.1. Calculations in different media

Optimized and experimental structures of di-hydrated tacrine can be observed in Fig. 2.

The optimizations with both methods and basis sets evidence strong changes in the positions of both water molecules, as observed in Fig. 3, although higher changes are observed in W2 than W1. Thus, W1 is bonded to H of NH while W2 is linked to Cl atom, as shown in Figs. 2 and 3. In the experimental structure, W2 is spatially distributed while the H atoms of W1 are in different positions. In the optimized structures with both methods one H–O bond of W2 is located practically planar to the rings while in W1 the two H present different positions, however, the O atom is practically in the same place.

In Table 1 are summarized calculated total E uncorrected and corrected by zero-point vibrational energy (E_{ZPVE}) together with the V and μ values for di-hydrated hydrochloride tacrine in the two media at different levels of theory.

Regarding the results, it is observed that the E and E_{ZPVE} values obtained with the wB97XD/6-311G* method in gas phase is approximately similar to predicted with the B3LYP/6-31G* method, as also was observed for ethylene oxide dimer [10]. Besides, the dipole moment value for the di-hydrated species considering the dispersion (20.07 D) is similar to observed for the anhydrous species (20.42 D) while the V in gas phase (288.1 $Å^3$) is comparable to predicted in aqueous solution with the B3LYP/6-31G* method, as in ethylene oxide dimer [10]. As expected, the di-hydrated tacrine present higher V and μ values than the anhydrous one due to the two water molecules. Also, the μ value rises from 19.82 D in the gas phase to 27.24 D in water. When the positions and directions of dipole moment vectors for di-hydrated and anhydrous tacrine are compared in Fig. 4 we observed few changes in the orientation and direction of vectors, however, higher variations in the magnitudes of those two species are observed.

3.2. Solvation energies

Here, the solvation energies of di-hydrated tacrine with both methods were predicted in aqueous solution because the presence of two water molecules could play a very important role in the properties of tacrine in solution. Hence, in Table 2 are presented corrected solvation energies by ZPVE and by the total non-electrostatic terms of anhydrous and di-hydrated hydrochloride tacrine in aqueous solution by using the B3LYP/6-311G* and wB97XD/6-311G* methods. Comparisons of these values with published for antiviral and laxative agents and for some alkaloids are also observed [1,26,28,31,32]. (ΔG_c) are calculated as the difference between the corrected solvation energies by ZPVE ($\Delta G^{\#}_{un}$) and by the non-electrostatic terms (ΔG_{ne}).

For example, for the B3LYP/6-311G* method the ΔG_{ZPVE} value is calculated as: −1226.9886 – (−1226.9236) Hartrees = −0.065 Hartrees x 627.51 kcal/mol = −40.78 × 4.18 = −170.49 kJ/mol. Then, the ΔG_{ne} value of 22.03 kJ/mol is obtained from of optimizations in solution using PCM calculations. These calculations show that the value of di-hydrated species (−192.52 kJ/mol) is slightly more negative than the anhydrous one and, hence, probably most soluble than that species (−162.02 kJ/mol) due obviously to the two water molecules. A very important resulted is that the solvation energy with both methods and basis sets are approximately the same. Comparisons with other hydrochloride antiviral or alkaloids agents, tacrine evidence higher values or most negative solvation energy values. However, high values are observed in the cationic species of those compared agents probably due to that the groups associated to tacrine are different from those related to amantadine. But, the value of di-hydrated species of tacrine is lower than the laxative sodium picosulphate due to the presence of two Na^+ and two SO_4^{2-} groups that increasing in notable form the solubility of that agent [32]. Hence, such changes justify the different biological activities observed in the compared species.

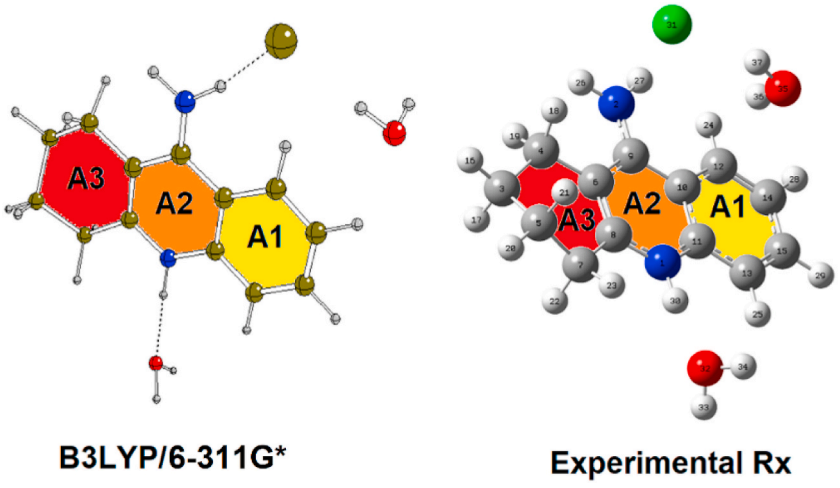

Fig. 2. Theoretical optimized structure and numbering of atoms for di-hydrated species of tacrine showing the intramolecular H-bonds with dashed lines (left) and experimental determined by X-ray diffraction (right) [13].

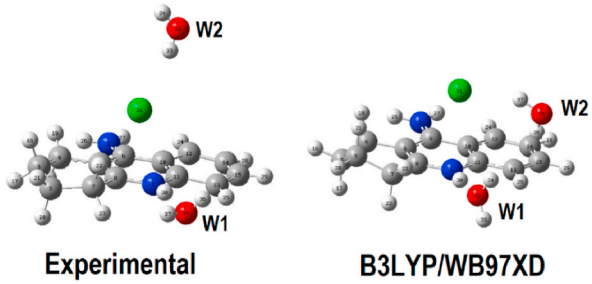

Fig. 3. Positions of two water molecules (W1 and W2) in the experimental and optimized structures of di-hydrated tacrine.

Table 1
Computed total (*E*), dipolar moment (μ) and volume (V) values of anhydrous and di-hydrated hydrochloride tacrine in both media by using the B3LYPand wB97XD methods and different basis sets.

HYDROCHLORIDE ANHYDROUS				
GAS PHASE				
Method	E (Hartrees)	E_{ZPVE} (Hartrees)	μ (D)	V (Å^3)
B3LYP/6-311G*	−1074.3185	−1074.0598	16.39	246.9
AQUEOUS SOLUTION				
B3LYP/6-311G*	−1074.3750	−1074.1155	20.42	248.7
HYDROCHLORIDE DI-HYDRATED				
GAS PHASE				
B3LYP/6-31G*	−1227.0177	−1226.7091	18.76	302.2
B3LYP/6-311G*	−1227.2323	−1226.9236	19.82	290.9
wB97XD/6-311G*	−1226.9658	−1226.6531	20.07	288.1
AQUEOUS SOLUTION				
B3LYP/6-31G*	−1227.0729	−1226.7650	24.03	288.1
B3LYP/6-311G*	−1227.2967	−1226.9886	27.24	289.8
wB97XD/6-311G*	−1227.0318	−1226.7182	26.88	288.4

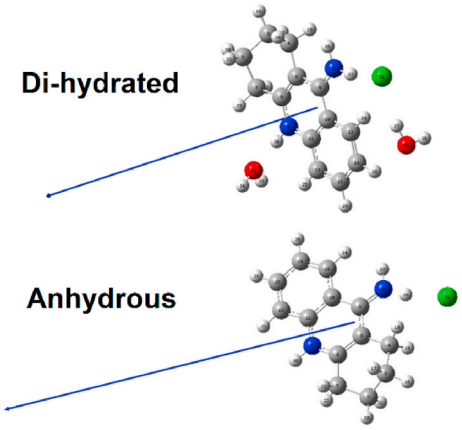

Fig. 4. Positions and orientations of dipole moment vectors for di-hydrated and anhydrous tacrine in solution by using B3LYP/6-311G* level of theory.

3.3. Structural parameters

Geometrical theoretical parameters for di-hydrated hydrochloride and anhydrous tacrine in the two media by using the B3LYP/6-311G* method are presented in Table 3 compared with the corresponding experimental determined by Moris et al. for di-hydrated hydrochloride tacrine [2]. The correlations between experimental and theoretical values are shown in the same table in terms of the root-mean-square deviation values (RMSD).

The optimized Cartesians coordinates of di-hydrated species of tacrine in gas phase and aqueous solution are shown in Tables S1 and S2 of supporting material. Reasonable correlations in the bond lengths are observed for the di-hydrated species in gas phase (0.135 Å) while in solution the value is closer to anhydrous one (0.070/0.069 Å). In relation to the bond angles, good concordances evidence the di-hydrated species, as expected because this form is similar to the compared one. The dihedral angles for the di-hydrated species in

Table 2
Corrected solvation energies by ZPVE ((kJ/mol) and by the total non-electrostatic terms of anhydrous and di-hydrated hydrochloride tacrine in aqueous solution by using different levels of theory.

HYDROCLORIDE TACRINE[a]			
B3LYP/6-311G* method[a]			
Species	ΔG_{ZPVE}	ΔG_{ne}	ΔG_c
ANHYDROUS	−146.10	15.92	−162.02
DI-HYDRATED	−170.49	22.03	−192.52
wB97XD/6-311G* method[a]			
DI-HYDRATED	−170.76	21.19	−191.95
B3LYP/6-31G* method[a]			
DI-HYDRATED	−146.62	22.99	−169.61
B3LYP/6-31G* method			
Sodium picosulphate[c]	−236.07	18.31	−254.38
Agents	Free base	Cationic	Hydrochloride
Amantadine[b]	−20.32	−273.24	−109.01
Morphine[b]	−60.91	−309.19	−144.74
Cocaine[b]	−71.26	−255.24	−138.14
Scopolamine[b]	−75.47	−310.34	−122.74
Heroin[b]	−88.67	−323.14	−161.94

[a] This work.
[b] From Ref [1,26,28,31].
[c] From Ref [32].

Table 3
Comparison of calculated geometrical parameters for the di-hydrated and anhydrous hydrochloride tacrine in both media by using the B3LYP/6-311G* method with the corresponding experimental in solid phase.

B3LYP/6-311G*[a]					
Parameters	DIHYDRATED		ANHYDROUS		Exp[b]
	Gas	Water	Gas	Water	
Bond lengths (Å)					
N1–H30	1.021	1.032	1.009	1.014	0.898
N1–C8	1.353	1.348	1.365	1.350	1.353
N1–C11	1.379	1.371	1.374	1.373	1.361
N2–H26	1.007	1.007	1.077	1.018	0.866
N2–H27	1.047	1.016	1.008	1.007	0.897
N2–C9	1.324	1.337	1.315	1.334	1.333
C9–C10	1.450	1.445	1.460	1.449	1.437
C9–C6	1.433	1.420	1.438	1.421	1.419
C6–C4	1.515	1.515	1.512	1.514	1.482
C10–C12	1.411	1.414	1.411	1.415	1.446
H27–Cl31[#]	2.027	2.385	1.898	2.363	2.401
RMSD	**0.135**	**0.070**	**0.172**	**0.069**	
Bond angles (°)					
H30–N1–C8	119.2	119.3	118.3	118.4	115.5
H30–N1–C11	117.8	117.7	118.2	118.0	121.7
C8–N1–C11	122.8	122.9	123.3	123.4	122.6
C6–C9–C10	118.7	119.1	118.5	119.1	118.9
N2–C9–C10	120.8	120.6	121.1	120.2	120.0
N2–C9–C6	120.4	120.1	120.2	120.5	121.0
H26–N2–H27	113.5	115.3	111.7	114.8	112.9
N2–H27–Cl31[#]	168.7	158.9	166.8	153.6	160.9
RMSD	**3.4**	**2.3**	**6.0**	**2.7**	
Dihedral angles (°)					
C9–N2–H27–Cl31[#]	−172.4	−167.2	154.4	179.6	−164.1
N2–C9–C6–C8	−176.3	−176.3	−175.2	−177.5	−176.9
N1–C8–C6–C4	179.9	−179.9	178.7	−179.7	178.9
N1–C11–C10–C12	−179.9	−179.7	−179.5	179.9	−179.9
N1–C8–C7–C5	161.5	161.6	163.9	161.9	164.5
N1–C11–C13–C15	−179.7	−179.9	179.7	−179.9	−165.9
RMSD	**6.7**	**146.6**	**191.9**	**250.5**	

[a] This work.
[b] Ref [2] for orthorhombic pseudopolymorph for tacrine hydrochloride.

gas phase presents a very good agreement (6.7°) however, in solution the dihedral N1–C8–C6–C4 shows signs change in this medium and, hence, low concordance are observed in these parameters, although a low value is observed for the di-hydrated species in solution (146.6°), as compared with the anhydrous one (250.5°). In the di-hydrated species, a clear enlargement of N2–H27 bond is evidenced as a consequence of Cl atom, hence, the distance of H27–Cl31 bond increasing from 2.027 Å in gas phase to 2.385 Å in solution while in the anhydrous species these values are slightly lower in both media, as observed in Table 3. Thus, the N1–H30 bond presents a lower value than N2–H27 bond and higher than the anhydrous species due to the presence of W1. Hence, this H bond of N1–H30 with the water molecule justify that Cl is linked to H of NH_2 group and not to H of N1–H30 group, as reported for the anhydrous species [1]. The good correlations observed in the geometrical parameters suggest that the vibrational assignments can be performed with the optimized structure of di-hydrated tacrine.

3.4. Charges, MEP and bond orders studies

Previously, for the hydrochloride anhydrous tacrine, the atomic charges, molecular electrostatic potential (MEP) and bond orders were studied to explain and understand why in the experimental structure the Cl atom is linked to H of NH_2 group instead H of NH [1]. Such observation was justified by the two water molecules bonded to Cl and to H of NH group. In this work, those properties were also analysed for the di-hydrated species and, later, compared with the obtained for anhydrous species. Therefore, atomic Merz-Singh-Kollman (MK), Mulliken (MU) and natural population (NPA) charges for di-hydrated species in the two media were computed with the B3LYP/6-311G* method. Table S3 shows those properties for the di-hydrated form of tacrine in both media while in Fig. 5 are presented the behaviours of three charges analysed for the anhydrous and di-hydrated species in the two media. Here, the analyses of the charges are presented only for those atoms involved in the H bond interactions with the two W1 and W2 water molecules. Those atoms are the related to A2 ring (see Figs. 1 and 2) which are, N1, N2, C6, C8, C9, C10, C11, H26, H27, H30 and Cl31. In general, it is observed the same behaviours for the three charges in the two media but, the exhaustive and detailed analyses show important differences in the three charges on H26, H27 and H30, as expected because these atoms belong to NH_2 and NH groups common to both anhydrous and di-hydrated species.

First, the three charges on N1 and N2 present different and negative values but the di-hydrated form in gas phase shows the same MK and NPA charges on N2. In the di-hydrated species, the three charges on H26 have similar values while the charges on H27 change slightly in solution. Besides, the three charges on H30 show higher and positive values while the three charges on Cl atom show the most negative values. In general, the NPA charges show higher values than the other ones.

When the MEP values are evaluated for both species from Table S3 [23], it is observed less negative MEPs values on H30 indicating that these atoms are the most labile in both species and media. Besides, the MEPs on Cl atoms slightly increase in the di-hydrated species in the two media than the anhydrous ones while the MEPs on H30 decrease in the di-hydrated species. Higher MEPs values are observed on N2 than N1 but lower value is observed in the di-hydrated species as compared with the other one. If the mapped MEP surfaces are analysed for the di-hydrated species in both media from Fig. 6, it is observed changes in the positions of water molecules

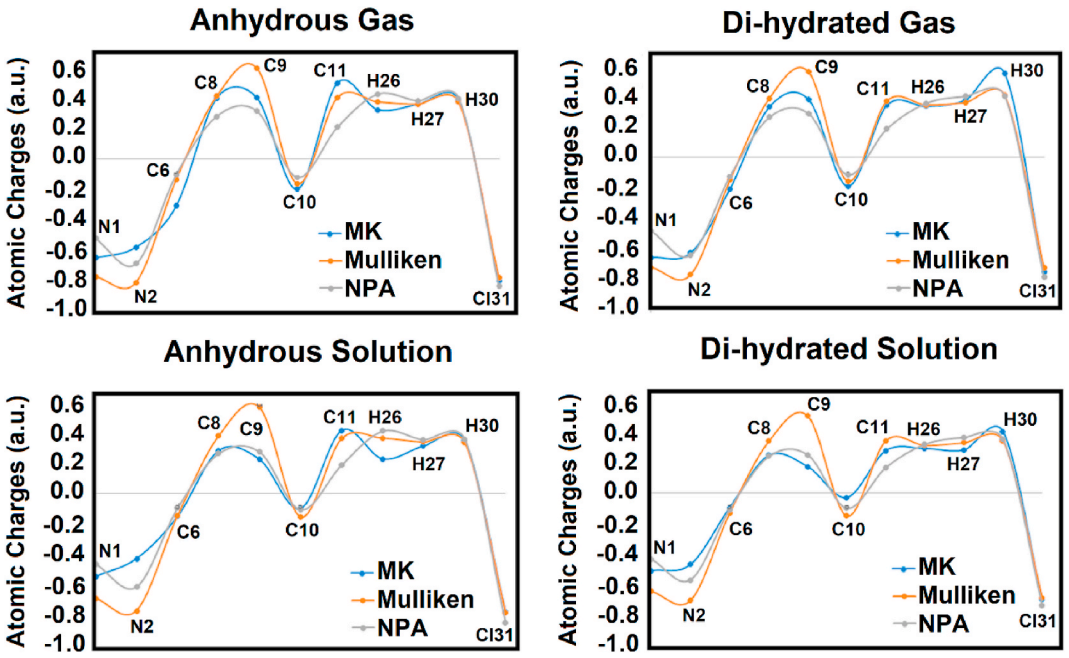

Fig. 5. Behaviours of atomic Merz-Singh-Kollman (MK), Mulliken and natural population (NPA) charges for the anhydrous and di-hydrated hydrochloride tacrine in gas phase and aqueous solution by using the B3LYP/6-311G* method.

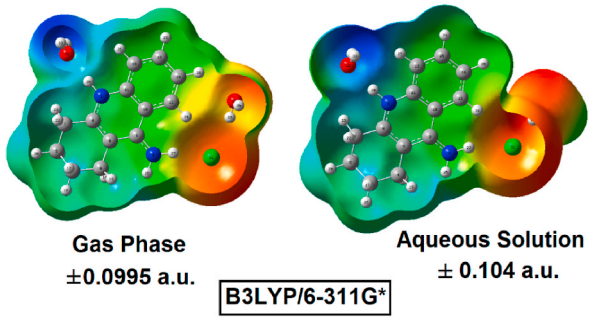

Fig. 6. Calculated electrostatic potential surfaces on the molecular surface of anhydrous and di-hydrated hydrochloride tacrine in gas phase and aqueous solution. B3LYP functional and 6-311G* basis set. Isodensity value of 0.005.

and in the colorations in solution. The di-hydrated species in solution shows strong colorations.

Hence, a lower MEP value is observed in gas phase (±0.0995 a. u.), as compared with the value in solution (±0.104 a. u.). This observation support the higher solvation energy value observed for the di-hydrated species (−192.52 kJ/mol) than the anhydrous one

Table 4
Main delocalization energies (in kJ/mol) for the anhydrous and di-hydrated hydrochloride tacrine in gas and aqueous solution phases by using B3LYP/6-311G* calculations.

B3LYP/6-311G* Method				
Delocalization	Di-Hydrated		Anhydrous	
	Gas	Water	Gas	Water
*πN1-C11 →π*C6–C8*		115.54		
*πC6-C8→π*N2–C9*	138.48		130.0816	149.0588
*πC10-C11→ π*N2–C9*	137.61		120.80	129.455
*πC10-C11→ π*C12–C14*	70.68		79.29	75.407
*πC10-C11→ π*C13–C15*	61.03		62.78	61.739
*πC12-C14→ π*C10–C11*	78.88	20.19	70.02	70.976
*πC12-C14→ π*C13–C15*	95.85	96.60	87.32	85.439
*πC13-C15→ π*N1–C11*	0.00	137.65		
*πC13-C15→ π*C10–C11*	92.04	0.00	89.87	90.163
*πC13-C15→ π*C12–C14*	61.49	58.90	68.59	67.925
$\Delta E_{\pi\rightarrow\pi^*}$	736.06	428.87	708.76	730.162
*LP(1)N2→ LP*C9*		669.13		
$\Delta E_{LP\rightarrow LP^*}$		669.13		
*πC6-C8→LP*C9*		234.12		
*πC12-C14→LP*C10*		196.84		
$\Delta E_{\pi\rightarrow LP^*}$		430.96		
*LP(1)N1→ σ*C6–C8*	207.66		173.47	187.93
*LP(1)N1→ σ*C10–C11*	177.61		179.24	179.49
*LP(1)Cl31→σ*N2–H26*	125.78	55.59	213.60	47.23
*LP(1)Cl31→σ*O35–H37*	32.52	37.03		
*LP(1)O32→σ*N1–H30*	52.58	73.02		
$\Delta E_{LP\rightarrow\sigma^*}$	596.15	165.65	566.31	414.66
*LP(1)C9→ π*C6–C8*		192.57		
*LP(1)C10→ π*N1–C11*		1082.54		
*LP(1)C10→ π*C12–C14*		218.70		
$\Delta E_{LP\rightarrow\pi^*}$		1493.81		
*π*N2–C9 →π*C6–C8*	330.97		261.46	285.954
*π*N2–C9 →π*C10–C11*	420.17		735.30	559.409
*π*N1–C11 →π*C6–C8*		164.19		
*π*N1–C11 →π*C13–C15*		286.16		
*π*C10–C11→ π*C12–C14*	307.77		712.23	587.457
*π*C10–C11→ π*C13–C15*	1041.36		1246.52	979.834
*π*C13–C14→ π*C12–C15*	372.81			
*π*C13–C15→ π*C12–C14*		379.79		
$\Delta E_{\pi^*\rightarrow\pi^*}$	2473.10	830.15	2955.51	2412.65
$\boldsymbol{\Delta E_{TOTAL}}$	**3805.30**	**4018.56**	**4230.58**	**3557.47**

[a]This work, Bold letters, total energy.

(−162.02 kJ/mol). Strong red colours are located on Cl31 and O35 of W2 while strong blue colours on H33 and H34 of W1. These sites indicate clear nucleophilic and electrophilic regions, respectively.

Then, the totals bond orders (BO) by atom, as Wiberg bond index, are examined for the di-hydrated species from Table S3. The results for all atoms of both species show few changes in the BO in solution, however, an important decreasing is observed in the Cl31 atoms of anhydrous species (from 0.328 in gas to 0.145 in water) while in the di-hydrated one few change is observed in the BO because it decreases from 0.291 to 0.224. Thus, the H bond of Cl31 to H37 of W2 justify the lower change. Important results are observed when the Wiberg bond index matrix in the NAO basis are analysed for the H27···Cl31, H30···O32 and H37···Cl31 bonds of di-hydrated species in both media. Thus, the BO of H27···Cl31 bond change from 0.1383 in gas to 0.082 in water, the BO of H30···O32 bond change from 0.0359 to 0.0551 while the BO of H37···Cl31 bond from 0.0393 to 0.052. Hence, the H27···Cl31 bond is weak compared to the H37···Cl31 bond, then, in solution the di-hydrated species is more strongly linked to two water molecules and, hence, the strong colorations observed in the MEP surface of this species in solution and, also, the higher solvation energy value of di-hydrated species.

3.5. NBO and AIM studies

To analyse the stabilities of the di-hydrated tacrine in both media two types of calculations were performed in this section because B3LYP/6-311G* calculations evidence that the di-hydrated tacrine in both media present two types of intra-molecular H bonds interactions. One of them, is between W1 and H30 of N1–H30 bond and the other one is formed between the H27 of NH_2 group and Cl31 but that expected between the Cl31 and O35 of W2 was not observed, as shown in Figs. 1 and 2. Hence, NBO and AIM calculations were performed for both species of hydrochloride tacrine [20–22]. Hence, Table 4 shows the donor-acceptor energy interactions computed with the NBO program for both species in the two media by using B3LYP/6-311G* [20].

Regarding Table 4, six different transitions were observed in those two species but three of them are only observed in solution while the other ones in the two media. Thus, the $\Delta E_{LP\rightarrow LP^*}$, $\Delta E_{\pi\rightarrow LP^*}$ and $\Delta E_{LP\rightarrow\pi^*}$ transitions observed in solution present high energy values and they are related to interactions between lone pairs of N2, C9 and C10 with antibonding orbitals of different N1–C11, C6–C8 and C12–C14 bonds of A1 and A2 rings, as can be seen in Table 4. The evaluation of total energy for both compared species shows a higher value for the anhydrous species in gas phase (4230.58 kJ/mol) while in solution the di-hydrated species present a higher E value (4018.56 kJ/mol). Hence, the di-hydrated species is the most stable in water due to its higher ΔG_c value. Then, the anhydrous species is the most stable in gas phase. Similar results were observed for rimantadine and amantadine [28,31].

NBO studies suggest that the di-hydrated species is most stable in solution due to three transitions not observed in the anhydrous one. Now, intra-molecular interactions in those two species are also analysed by means of the topological properties computed in the bond critical points (BCPs) and ring critical points (RCPs) with the AIM 2000 program [21,22]. Hence, the electron density, the Laplacian values and the $|\lambda 1|/\lambda 3$ ratio are computed in both media. The $|\lambda 1|/\lambda 3$ ratios are calculated with the eigenvalues of the Hessian matrix $(\lambda 1, \lambda 2, \lambda 3)$. In Table S4 are presented those properties for the di-hydrated and anhydrous hydrochloride species of tacrine in both media at the B3LYP/6-311G* level of theory. The distances involved in new H bonds are also presented in the table. We know that the interaction is ionic or polar covalent if the ratio $\lambda 1/\lambda 3 < 1$ and $\nabla^2\rho(r) > 0$ (closed-shell interaction). Fig. 7 shows details of the molecular models for the di-hydrated species in gas phase and solution by using B3LYP/6-311G* level of theory. The graphics

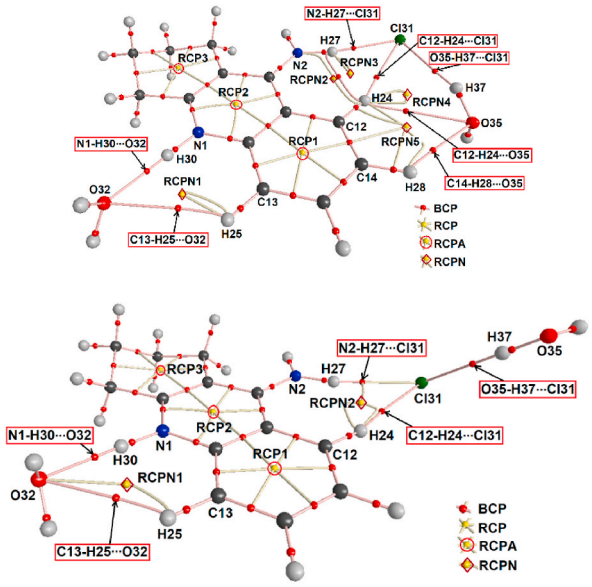

Fig. 7. Details of the molecular models for the di-hydrated hydrochloride tacrine in gas phase (upper) and aqueous solution (bottom) showing the geometries of all their bond critical points (BCPs) and ring critical points (RCPs) at the B3LYP/6-311G* level of theory.

show clear differences in the number and characteristics of interactions. Thus, in gas phase are observed seven interactions (N1–H30···O32, N2–H27···Cl31, C12–H24···Cl31, C12–H24···O35, C13–H25···O32, C14–H28···O35 and O35–H37···Cl31) while in solution only five H bonds interactions. RCPA correspond to the RCP of A1, A2 and A3 rings while RCPN to the new RCP formed as consequence of H bonds.

Thus, the N1–H30···O32, N2–H27···Cl31, C12–H24···Cl31, C13–H25···O32, and O35–H37···Cl31 interactions are observed in solution. Previous NBO results evidenced that the di-hydrated species in gas phase is less stable than in solution (total energy = 3805.30 kJ/mol) while this AIM study support the higher stability of di-hydrated species in gas phase due to the seven H bonds interactions, a resulted different from obtained from NBO study. Table S2 shows that, (i) for the A1 ring the properties present higher values than the other ones, (ii) the N1–H30···O32 and N2–H27···Cl31 interactions have higher topological properties in gas phase while in solution change to the N1–H30···O32 and O35–H37···Cl31 interactions. Note that the new interactions in the two media present lower distances between its two involved atoms. The lower number of H bonds interactions obtained for the di-hydrated species in solution compared to that obtained in the gas phase suggests that this species is more stable in the gas phase and, less stable in solution.

Probably, the difference observed in the different MEP values (higher in gas phase) and in the colorations observed on surfaces justify the different results from NBO and AIM studies.

3.6. Frontier orbitals

The anhydrous hydrochloride tacrine presents in gas phase and aqueous solution high reactivities in gas phase and water due to its low gap values calculated from the differences between the HOMO-LUMO (2.4572 and 1.3877 eV) [1]. In this work, the effect of two water molecules on gap values and descriptors for the di-hydrated species in both media at different levels of theory are analysed. In particular, the influence of the B3LYP and wB97XD methods and of 6–31G* and 6-311G* basis sets are also evaluated. Table 5 shows the calculated HOMO, LUMO and gap values together with the chemical potential (μ), electronegativity (χ), global hardness (η), global softness (S) and global electrophilicity index (ω) descriptors compared with values predicted for some hydrochloride antiviral agents such as, rimantadine, adamantadine and oseltamivir and, alkaloid as hydrobromide of scopolamine [26,28,31,33].

Note that the equations used to calculate the descriptors are also presented in Table 5. Comparisons between HOMO-LUMO and

Table 5
HOMO and LUMO, gap values and descriptors for the anhydrous and di-hydrated hydrochloride tacrine in gas phase and aqueous solution by using different levels of theory.

Tacrine[a]								
Orbital	Di-hydrated						Anhydrous	
	B3LYP/6-311G*		B3LYP/6-31G*		wB97XD/6-311G*		B3LYP/6-311G*	
	Gas	Water	Gas	Water	Gas	Water	Gas	Water
HOMO	−5.3253	−5.0586	−4.9824	−4.5742	−7.4967	−7.1403	−5.0314	−4.3048
LUMO	−2.0545	−2.5279	−1.8204	−2.2694	−0.2667	−0.8163	−2.5742	−2.9171
|GAP|	3.2708	2.5307	3.1620	2.3048	7.2300	6.3240	2.4572	1.3877
DESCRIPTORS								
χ	3.6899	3.79325	3.4014	3.4218	3.8817	3.9783	3.8028	3.6110
μ	−3.6899	−3.79325	−3.4014	−3.4218	−3.8817	−3.9783	−3.8028	−3.6110
η	1.6354	1.26535	1.581	1.1524	3.615	3.1620	1.2286	0.6939
S	0.3057	0.3951	0.3163	0.4339	0.1383	0.1581	0.4070	0.7206
ω	4.1627	5.6857	3.6589	5.0801	2.0840	2.5027	5.8853	9.3961
Antiviral							Alkaloid	
B3LYP/6–311++G** Method							B3LYP/6-31G*	
Orbital	Rimantadine[b]		Amantadine[c]		Oseltamivir[d]		Scopolamine[e]	
	Gas	Water	Gas	Water	Gas	Water	Gas	Water
HOMO	−6.3374	−5.3827	−6.3294	−6.4736	−6.7375	−6.9906	−5.3908	−5.0022
LUMO	−0.9338	−1.1937	−0.9334	−0.4218	−1.4558	−1.6245	−0.4669	0.4004
|GAP|	5.4036	4.1890	5.3960	4.1116	5.2817	5.3661	4.9239	5.4026
DESCRIPTORS								
χ	−2.7018	−2.0945	−2.6980	−2.0558	−2.6409	−2.6830	−2.4620	−2.7013
μ	−3.6356	−3.2882	−3.6314	−3.3130	−4.0967	−4.3075	−2.9289	−2.3009
η	2.7018	2.0945	2.6980	2.0558	2.6409	2.6830	2.4620	2.7013
S	0.1851	0.2387	0.1853	0.2432	1.3204	1.3415	0.2031	0.1851
ω	2.4461	2.5812	2.4439	2.6695	3.1775	3.4578	1.7421	0.9799

6From Ref. [26], χ = - [E(LUMO)- E(HOMO)]/2; μ = [E(LUMO) + E(HOMO)]/2; η = [E(LUMO) - E(HOMO)]/2; S = ½η; ω = μ2/2η.

[a] This work.
[b] From Ref [28].
[c] From Ref [31].
[d] From Ref [33].

Gap energies of anhydrous and di-hydrated hydrochloride tacrine in both media and at different levels of theory are shown in Fig. S1. Regarding the figure, it is observed that the higher gap values and lower HOMO energy are observed for the di-hydrated species in both media with the wB97XD/6-311G* method (grey colour) and the lower gap values for the anhydrous (yellow colour) while the B3LYP/6-311G* and B3LYP/6-31G* methods show few differences in the values. Thus, taking into account all employed methods the anhydrous species is the most reactive than the di-hydrated one in the two media. Moreover, comparing with the other antiviral and alkaloid species both forms of tacrine are most reactive, with exception of values calculated with the wB97XD/6-311G* method. Analysing the descriptors, it is observed that when the value of global electrophilicity index (ω) is high (9.3961 eV) a lower gap is observed for the anhydrous species of tacrine (1.3877 eV). Thus, probably that descriptor has influence on reactivity in both media. This study show the clear influence of method and basis set on the gap and descriptor values of the two tacrine species. Thus, the B3LYP method with both 6-311G* and 6-31G* basis sets predict similar gap values but different from obtained with the wB97XD/6-311G* method. In addition, the two water molecules decrease the reactivity of di-hydrated hydrochloride tacrine probably because it is hydrated.

3.7. Vibrational study

B3LYP/6-311G* and wB97XD/6-311G* calculations have optimized the structures of di-hydrated hydrochloride tacrine with C_1 symmetries, as in the anhydrous species although the number of normal vibration modes increases from 87 in the anhydrous species to 105 in the di-hydrated due to the two water molecules. Fig. 8 displays a comparison of experimental IR spectrum of tacrine in the solid state with the predicted for the di-hydrated and anhydrous species in water because better relationships are observed with these spectra [29]. Fig. 8 shows the IR spectra predicted with both methods. Fig. 9 show comparisons between the experimental Raman spectra of tacrine in the solid state with the corresponding predicted for the di-hydrated and anhydrous species in water [29]. Reasonable correlations among the predicted Raman spectra with both methods can be seen when the activities are transformed to intensity [30].

Fig. S2 shows comparisons between the experimental infrared spectrum with the corresponding predicted in gas phase for both species while in Fig. S3 are compared the predicted infrared spectra for the anhydrous and di-hydrated species in gas phase by using the B3LYP/6-311G* method. Few bands can be observed in the predicted IR spectra for the two species in gas phase while higher quantity of bands are observed in solution. Both, IR and Raman spectra in the gas phase were predicted for the isolated molecule where the packing forces are not considered and, for this reason, both spectra in solution show better correlations with the experimental one due to the H bonds interactions. A very important observation obtained from calculations is that both methods predict different assignments, as can be quickly seen from *GaussView* program [24]. Complete assignments of di-hydrated species were performed with the SQMFF methodology by using the Molvib program, transferable scaling factors and the normal internal coordinates [11–13]. Table 6 shows observed and calculated wavenumbers and assignments for di-hydrated and anhydrous hydrochloride tacrine in gas phase.

Previously, the IR and Raman bands between 2827/2686 and 720/693 cm^{-1} regions confirm the presence of cationic species of tacrine in the solid phase [1] but bands assigned to di-hydrated species are also assigned in that latter region, as detailed in Table 6. Some assignments are discussed below by main regions.

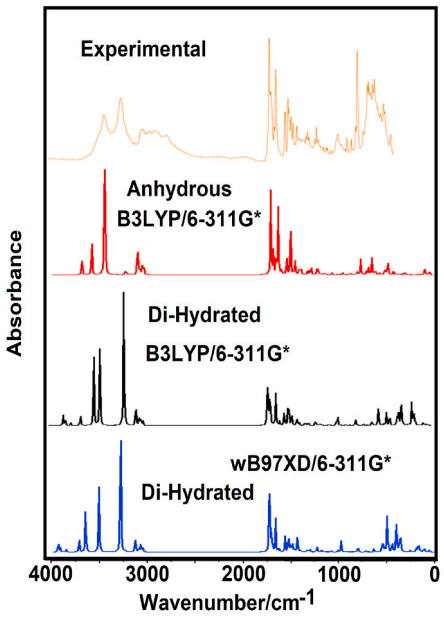

Fig. 8. Comparison between the experimental Infrared spectrum of hydrochloride tacrine in solid phase [29] with the predicted for anhydrous and di-hydrated hydrochloride tacrine in aqueous solution by using B3LYP/6-311G* and wB97XD/6-311G* methods.

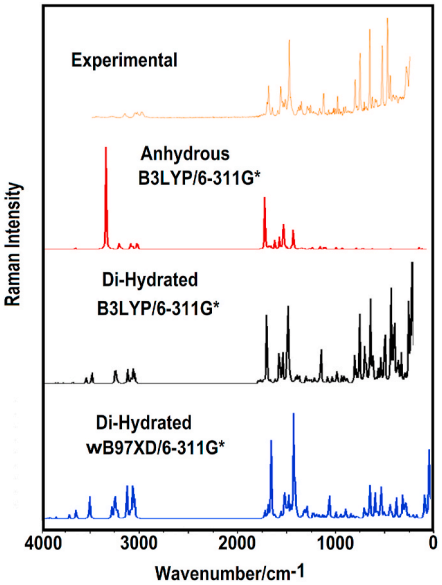

Fig. 9. Comparison between the experimental Raman spectrum of hydrochloride tacrine in solid phase [29] with the predicted for anhydrous and di-hydrated hydrochloride tacrine in aqueous solution by using B3LYP/6-311G* and wB97XD/6-311G* methods.

3.7.1. 4000-2000 cm^{-1} region

The wB97XD/6-311G* method predict the two antisymmetric and symmetric stretching modes of water molecules between 3821 and 3565 cm^{-1} different from the B3LYP/6-311G* one (3692 and 3583 cm^{-1}). In trehalose, these modes are also predicted in these regions [14]. Here, it is very important clarify that these bands were not observed in the experimental IR spectra reported by Sorrenti el at for the mono and di-hydrated species of tacrine [34]. Hence, the shoulder and IR band at 3378 and 3330 cm^{-1} can be assigned to the stretching modes of two water molecules, to the expected NH_2 stretching modes and to N1–H30 stretching modes [1,14,30,31]. Here, the B3LYP/6-311G* method predict a symmetric NH_2 stretching mode at 2702 cm^{-1} while the other method at 2904 cm^{-1}, thus, the IR band at 2700 cm^{-1} is assigned to that vibration mode. Previously, the very weak band at 2250 cm^{-1} was assigned to N1–H30 stretching mode of hydrochloride form I while the band at 2319 cm^{-1} was assigned to symmetric NH_2 stretching mode predicted at 2365 cm^{-1} [1]. The group of IR and Raman bands and shoulders between 3163 and 2886 cm^{-1} are assigned to the different stretching modes of CH_2 and C–H groups of both species of tacrine [1,14,30,31].

3.7.2. 1800–1000 cm^{-1} region

In this region, the deformations modes of two water molecules are predicting by two methods practically in the same positions while the deformation mode of NH_2 group at different wavenumbers. In trehalose, these deformation modes corresponding to the two water molecules are predicted by B3LYP/6-31G* calculations at 1660 and 1623 cm^{-1} and assigned to the IR bands at 1687 and 1639 cm1 [14]. Hence, the strong IR bands at 1665 and 1615 cm^{-1} are assigned to deformation modes of two water molecules while the bands at 1665 and 1650 cm^{-1} can be assigned to NH_2 deformation modes [1,26,28,31]. In the anhydrous species that mode is assigned to 1665 cm^{-1}. Note that the C═C, C–C and C–N stretching modes, wagging and rocking CH_2 modes of di-hydrated species are predicting by two methods in approximately the same regions but in different positions, as detailed in Table 6. The NH_2 rocking mode of di-hydrated species is predicted by the two methods coupled with other modes between 1139 and 1112 cm^{-1} while in anhydrous species that mode is predicted as a pure mode at 1107 cm^{-1}.

3.7.3. 1000–10 cm^{-1} region

In this region are expected the libration modes of water molecules and, in addition, to twisting and wagging modes of CH_2 and NH_2 together with other modes such as, C–C stretching modes, out-of-plane CH deformations and deformations and torsions of three rings. From Figs. 1 and 2 we observed that the O32 of W1 is bonded to N1–H30 bond while the Cl31 is linked to H37 of O35–H37 of W2 and, for these reasons, only the libration modes of W1 can be assigned in Table 6. These modes are identified as rocking, ρH_2O(W1); wagging, $wagH_2O$(W1) and twisting, τwH_2O(W1) modes. In the di-hydrated species of trehalose these modes are assigned to 451/308, 288/276 and 538 cm^{-1}, respectively [14] while in the di-hydrated species of tacrine the ρH_2O(W1), $wagH_2O$(W1) and τwH_2O(W1) modes are predict by the two methods coupled with other skeletal modes at 294/289, 212/196 and 264/140 cm^{-1}, respectively. The twisting modes of W1 are also predict coupled with torsion modes of W2 (τH27-Cl31,τwN2-H27) at lower wavenumbers between 54 and 22 cm^{-1}. The $wagNH_2$ and τwNH_2 vibration modes are assigned to the IR band of medium intensity at 540 cm^{-1}, as predict by two calculations. In Table 6 can be seen the assignments of remains vibrational modes.

Table 6
Observed and calculated wavenumbers (cm^{-1}) and assignments for the di-hydrated and anhydrous hydrochloride tacrine.

Hydrochloride tacrine							
Experimental[c]		B3LYP/6-311G* Method[a]		wB97XD/6-311G* Method[a]		Anhydrous[d]	
IR	Raman	SQM[b]	Assignments[b]	SQM[b]	Assignments[b]	SQM[b]	Assignments[d]
		3692	ν_aH_2O(W1)	3821	ν_aH_2O(W1)		
		3632	ν_aH_2O(W2)	3750	ν_aH_2O(W2)		
				3712	ν_sH_2O(W1)		
		3583	ν_sH_2O(W1)	3565	ν_sH_2O(W2)		
3378sh		3494	ν_aNH_2	3545	ν_aNH_2		
3378sh		3380	ν_sH_2O(W2)			3486	ν_aNH_2
3330 m	3277vw	3278	νN1-H30	3324	νN1-H30	3462	νN1-H30
3163s	3242vw	3088	νC14-H28	3090	νC14-H28	3072	νC14-H28
3089sh	3098vw	3072	νC13-H25	3084	νC13-H25	3060	νC15-H29,νC12-H24
3067sh		3057	νC15-H29	3075	νC12-H24	3051	νC14-H28,νC12-H24, νC15-H29
		3051	νC12-H24	3064	νC15-H29		
		2971	ν_aCH_2(C5)	2989	ν_aCH_2(C3)		
3028vw		2968	ν_aCH_2(C3)	2986	ν_aCH_2(C5)	3034	νC13-H25
	2971w	2954	ν_aCH_2(C7)	2976	ν_aCH_2(C7)	2962	ν_aCH_2(C3)
2950 m		2926	ν_sCH_2(C3)	2945	ν_aCH_2(C4)	2956	ν_aCH_2(C4)
2924 m		2920	ν_sCH_2(C5)	2933	ν_sCH_2(C5)	2953	ν_aCH_2(C5)
		2910	ν_aCH_2(C4)	2925	ν_sCH_2(C3)	2923	ν_sCH_2(C4)
		2901	ν_sCH_2(C7)	2923	ν_sCH_2(C7)	2919	ν_sCH_2(C5)
2888sh		2881	ν_sCH_2(C4)	2904	ν_sNH_2	2905	ν_aCH_2(C7)
	2871w	*2885*	*ν_aCH_2(C3) Cationic*[d]	2900	ν_sCH_2(C4)	2892	ν_sCH_2(C3)
2866 m		*2869*	*ν_sCH_2(C5) Cationic*[d]			2881	ν_sCH_2(C7)
	2851w	*2855*	*ν_sCH_2(C3) Cationic*[d]				
2827 m	2807w	*2822*	*ν_sCH_2(C4) Cationic*[d]				
2792 m	2794sh	*2762*	*ν_sCH_2(C7) Cationic*[d]				
2700 m	2757vw	2702	ν_sNH_2				
2319vvw	2333vvw					2365	ν_sNH_2
2250vvw		*2172*	*νN1-H30 Form I*				
1665vs		1666	$\delta_{H2}O$(W2)	1685	$\delta_{H2}O$(W2)	1627	δNH$_2$,βN1-H30
1665vs		1654	δNH$_2$,δN2-H27-Cl31	1682	τwH30-N1	1626	δNH$_2$
1650s		1648	βN1-H30	1664	δNH$_2$,δN2H27Cl31		
1615s	1573 m	1623	$\delta_{H2}O$(W1)	1645	$\delta_{H2}O$(W1)	1594	νC13-C15,βN1-H30
1600s	1562s	1605	νC13-C15	1634	νC13-C15	1586	νC6-C8
1506s	1523w	1598	νC6-C8	1621	νC6-C8	1531	νC6-C8,νN1-C8
1475s	1475w	1541	νN1-C8	1567	νN1-C8,νC6-C8	1499	νN2-C9
1466s	1468w	1506	νN2-C9	1517	νN2-C9,δN2H27Cl31	1466	βC12-H24
1459 m		1483	βC12-H24	1500	νN2-C9,βC12-H24	1450	δCH$_2$(C5)
1442s	1442s	1465	δCH$_2$(C5),δCH$_2$(C4)	1463	δCH$_2$(C5)	1444	δCH$_2$(C3)
	1438sh	1455	δCH$_2$(C5),δCH$_2$(C3)	1458	τwH30-N1,δCH$_2$(C5)	1438	βC15-H29,βC14-H28
1420 m	1425w	1450	δCH$_2$(C4)	1455	δCH$_2$(C3)	1418	δCH$_2$(C7)
1416sh	1411w	1446	τwH30-N1,τwH$_2$O(W1)	1446	νC6-C9	1414	wagCH$_2$(C4), νC6-C9
1386 m	1386w	1433	δCH$_2$(C7)	1439	δCH$_2$(C4)	1408	δCH$_2$(C4)
1375sh	1372sh	1426	νC6-C9	1423	δCH$_2$(C7)	1380	wagCH$_2$(C7), wagCH$_2$(C4)
1363sh		1387	wagCH$_2$(C3),wagCH$_2$(C7)	1392	wagCH$_2$(C7)	1363	wagCH$_2$(C3)
1350sh	1355vs	1368	wagCH$_2$(C3)	1380	wagCH$_2$(C3)	1355	wagCH$_2$(C5)
	1346sh	1366	wagCH$_2$(C5),wagCH$_2$(C7)	1371	wagCH$_2$(C5),νC5-C7	1345	wagCH$_2$(C7)
1322w	1333sh	1354	wagCH$_2$(C4),νC11-C13	1361	νC10-C11,νC12-C14	1331	νC10-C11,νC12-C14
1307w		1346	νC10-C11,νC9-C10	1356	wagCH$_2$(C4),νC9-C10	1296	ρCH$_2$(C4), ρCH$_2$(C5)
1294w		1302	βC13-H25	1313	βC13-H25, wagCH$_2$(C7)	1280	βR$_1$(A2)
1276 m	1274w	1287	βR$_1$(A2)	1300	βR$_1$(A2)	1258	ρCH$_2$(C7), ρCH$_2$(C4)
1261w	1250w	1267	τwH30-N1,τwH$_2$O(W1)	1275	νN1-C8	1247	νN1-C11,νC10-C12
	1239w	1253	ρCH$_2$(C4),νN1-C11,νC10-C12	1263	ρCH$_2$(C7)	1224	νN1-C8
1207w	1217sh	1247	ρCH$_2$(C7),ρCH$_2$(C3)	1257	νN1-C11,νC10-C12		
1186 m	1180w	1190	βC14-H28,νC4-C6	1204	νC4-C6	1185	ρCH$_2$(C5),ρCH$_2$(C3)
1169w		1181	βC14-H28,ρCH$_2$(C5)	1191	βC14-H28	1177	βC14-H28
	1160w	1161	βC13-H25,βC15-H29	1166	βC13-H25,νC11-C13 βC15-H29	1159	βC15-H29,βC13-H25
1147w	1145w	1142	ρCH$_2$(C5)	1156	ρCH$_2$(C5),ρCH$_2$(C3)	1145	ρCH$_2$(C3), ρCH$_2$(C5)
1138sh	1138sh	1136	ρNH$_2$,βR$_1$(A3)	1139	ρNH$_2$		
						1119	νC9-C10,νC11-C13
1114w	1117w	1112	ρNH$_2$,δN2H27Cl31	1120	ρNH$_2$,δN2H27Cl31	1107	ρNH$_2$
1086w	1097w	1088	νC7-C8	1095	νC7-C8	1081	νC7-C8
1078w	1062sh	1052	γC14-H28	1084	γC14-H28,γC12-H24		
1038w	1056w	1048	νC3-C5	1059	νC3-C4	1042	νC3-C5,νC3-C4

(*continued on next page*)

Table 6 (*continued*)

Hydrochloride tacrine							
Experimental[c]		B3LYP/6-311G* Method[a]		wB97XD/6-311G* Method[a]		Anhydrous[d]	
IR	Raman	SQM[b]	Assignments[b]	SQM[b]	Assignments[b]	SQM[b]	Assignments[d]
1012sh	1018s	1024	νC14-C15,νC12-C14	1030	νC14-C15	1022	νC14-C15
		1016	τwCH$_2$(C4),τwCH$_2$(C3),τwCH$_2$(C5) τwCH$_2$(C7)	1023	τwCH$_2$(C5),τwCH$_2$(C3)	1010	τwCH$_2$(C5),τwCH$_2$(C3), τwCH$_2$(C7)
1000sh	994w					*1008*	*νC13-C15,νC14-C15*[d]
985sh	970w	975	γC15-H29,γC12-H24,γC13-H25	1003	τH27-Cl31,τwN2-H27	975	γC15-H29,γC14-H28
973 m		962	νC5-C7,νC3-C4	976	τH27-Cl31,τwN2-H27	964	νC5-C7,νC3-C4
966sh	960w			975	τH27-Cl31,τwN2-H27	941	τwN2-H26,wagNH$_2$
946sh	940vw	922	τH27-Cl31			927	γC12-H24
900vw	918w	904	βR$_1$(A1)	910	βR$_1$(A1)	899	βR$_1$(A1)
880 m	885s					866	βR$_1$(A3)
874sh	868w	883	τH27-Cl31,τwN2-H27	905	τH27-Cl31,τwN2-H27		
	848w	869	βR$_1$(A3)	891	τwH30-N1,τH27-Cl31	852	νC3-C5
836 m						843	γC13-H25
	827w					832	τwCH$_2$(C4)
793sh	805w	861	τwH30-N1,τwH$_2$O(W1)	879	βR$_1$(A3)	793	τR$_1$(A2)
776vs	778w	851	τwH30-N1,τwH$_2$O(W1)	868	νC3-C5	783	γC9-N2,τR$_1$(A2)
760sh	760w	844	τwH30-N1,τwH$_2$O(W1)	852	τwCH$_2$(C4),τwCH$_2$(C7)	754	γC15-H29,τwCH$_2$(C4)
	744w	796	δN2H27Cl31	805	τR$_1$(A2)	741	τR$_1$(A3), γC14-H28
	720sh	788	τH27-Cl31,τwN2-H27	796	δN2H27Cl31		
717 m	710s	774	τR$_1$(A2)	792	γC13-H25,γC15-H29		
	693w	751	τR$_1$(A3)	771	τR$_1$(A3)		
676s	679vw	695	τR$_1$(A3),νC4-C6	706	τR$_1$(A3),γC9-N2	693	τR$_1$(A3), νC4-C6
662s	662s	674	γC9-N2	690	τR$_1$(A3),γC9-N2	670	τR$_1$(A3)
643s	650sh	658	βR$_3$(A3)	665	βR$_3$(A3)	656	βR$_3$(A3)
621s	621w	625	τCl31-H37,τH37-O35	618	βR$_2$(A3)	603	βR$_2$(A3)
604s	601w	605	βR$_2$(A3)	601	δN2H27Cl31,βC9-N2	601	γC9-N2
573sh	576sh	596	βC9-N2,δN2H27Cl31	599	τCl31-H37	567	βR$_3$(A3), τ$_w$NH$_2$
	566vs	554	βR$_3$(A3)	563	τ$_w$NH$_2$,τH27-Cl31	555	γN1-H30
540 m	539w	537	τwNH2,wagNH2	552	τ$_w$NH$_2$,wagNH$_2$	536	γN1-H30,τR$_2$(A2)
511s	511w	519	τR$_3$(A3)	526	τR$_3$(A3)	523	τR$_3$(A3)
499s	499w	499	βR$_3$(A1),βR$_3$(A2)	505	βR$_3$(A1),βR$_3$(A2)	497	βR$_3$(A1),βR$_3$(A2)
487sh	492sh	480	δN2H27Cl31	486	δN2H27Cl31,βR$_2$(A1)	483	βR$_2$(A1),βR$_1$(A1)
444 m	444s	431	τR$_2$(A3),ButC10-C11	439	τR$_2$(A3),ButC10-C11		
422sh	427sh	426	βR$_2$(A2),βR$_2$(A1)	430	βR$_2$(A2),βR$_2$(A1)	424	βR$_2$(A2)
	407sh	369	βR$_3$(A1),δN2H27Cl31	373	βR$_3$(A1)	416	τR$_2$(A3), ButC10-C11
	391vs	354	βC9-N2	346	βC9-N2	366	βR$_2$(A2),βC9-N2
	367s	317	τR$_1$(A1),τR$_2$(A2),γN1-H30	325	τR$_1$(A1),γN1-H30	357	βC9-N2
	336w	295	ButC6-C8	301	τR$_3$(A1)		
	309w	289	ρH$_2$O(W1)	294	ButC6-C8,ρH$_2$O(W1)	309	τR$_1$(A1)
	299sh	284	δCl31H37O35	264	τwH$_2$O(W1), τwH30-N1	286	ButC6-C8
	284sh	263	τwH$_2$O(W1),τwH30-N1	243	βR$_2$(A1),νH27-Cl31		
	273sh	239	βR$_2$(A1),νH27-Cl31	239	τCl31-H37,τwN2-H27		
	265w	212	wagH$_2$O(W1)	196	wagH$_2$O(W1)	265	τR$_3$(A1),τR$_2$(A2)
	242w	205	τH27-Cl31,τH37-O35	178	δCl31H37O35	226	βR$_2$(A1)
	206s	168	νH37-Cl31	173	νO32-H30	173	νH26-Cl31
		161	τR$_2$(A1)	159	τwN2-H27,τR$_2$(A1)		
	173sh	159	τwN2-H27,τH27-Cl31	150	νH37-Cl31,νH27-Cl31	156	τR$_2$(A1)
		149	νH27-Cl31,νO32-H30	145	τwN2-H27		
		140	τwH$_2$O(O32)	143	νH37-Cl31, δCl31H37O35		
		133	τwN2-H27	141	τwN2-H27, τwH$_2$O(W1)		
		108	τR$_3$(A2),τR$_3$(A1)	108	τR$_3$(A2)	113	ButC6-C8,τR$_3$(A1)
		106	τH27-Cl31,τwN2-H27	106	τH27-Cl31,τwN2-H27	99	τR$_3$(A2)
		69	δ_H27Cl31H37,δN2H27Cl31	70	τR$_2$(A2),τR$_2$(A1)	71	δN2-H26-Cl31
		67	δ_H27Cl31H37	64	δ_H27Cl31H37		
		52	τwH30-N1	54	τwH30-N1, τwH$_2$O(W1)	54	τR$_2$(A2), τ$_w$NH$_2$
		43	τwH30-N1,τwH$_2$O(W1), **δN1H30O32**	42	τwN2-H27,τwH30-N1 **N1H30O32**		
		28	τH27-Cl31,τwN2-H27	29	τH27-Cl31		
		23	τwN2-H27,τwH$_2$O(W1)	22	τwH$_2$O(W1), τwH30-N1	16	wagNH$_2$ τwN2-H26,τ$_w$NH$_2$

Abbreviations: ν, stretching; β, deformation in the plane; γ, deformation out of plane; wag, wagging; τ, torsion; β$_R$, deformation ring τ$_R$, torsion ring; ρ, rocking; τw, twisting; δ, deformation; a, antisymmetric; s, symmetric; (A$_1$), Ring1; (A$_2$), Ring2; (A$_3$), Ring3.

[a] This work.

[b] From scaled quantum mechanics force field.
[c] From Ref [29].
[d] From Ref [1]. Italic letters, Ref [1], Bold letters, from *GaussView*.

4. Force constants

Harmonic scaled force constants for the di-hydrated hydrochloride tacrine in gas phase were computed with both methods from the SQMFF methodology and the Molvib program [11–13]. These parameters can be seen in Table 7 compared with the corresponding to the anhydrous species, the antivirals rimantadine and amantadine, the alkaloid hydrobromide of scopolamine and, to the sugar non reducing disaccharide of glucose, trehalose [1,14,26,28,31]. Different methods used are indicated in Table 7.

Regarding exhaustively all the force constants values, we observed that the wB97XD method predict higher force constants values than the B3LYP one with exception of constant of CH_2 deformation which presents practically the same value. Comparing the force constants of di-hydrated and anhydrous species, it is observed slightly lower values of all constants except for the *f(νN-H)* force constant because the W1 water molecule kinked to H30 of N1–H30 bond decrease the frequency of N1–H30 stretching mode in the di-hydrated (see Table 6) and, hence, the value of that force constant is higher in the anhydrous species. Comparing the values with trehalose, it is observed lower *f(νO-H)* force constant for the sugar due probably to different B3LYP/6-31G* method used. The remaining force constants of trehalose have approximately similar values to tacrine due to that this sugar is di-hydrated as tacrine. Note that the *f(νO-H)* force constant for scopolamine is similar to tacrine despite this alkaloid presents one OH group instead one water molecule. The differences in the values observed with the antiviral agents are related not only to the structure and method used but to its fused rings different from tacrine, as can be seen in Fig. S4. The structures of anhydrous and di-hydrated species are observed in Figs. 1 and 2.

5. NMR study

The GIAO and hybrid B3LYP/6-311G* and wB97XD/6-311G* methods were used to predict ^1H and ^{13}C NMR chemical shifts of di-hydrated and anhydrous hydrochloride tacrine. Comparisons of predicted chemical shifts with the corresponding experimental of anhydrous tacrine in D_2O and monohydrate in polysol [29], respectively are summarized in Tables 8 and 9. Correlations between experimental and predicted chemical shifts are presented in terms of RMSD values.

Better correlations for the ^1H nucleus are observed for the anhydrous species when the predicted values are compared with the experimental obtained for this species (0.2 ppm) while when the values for the di-hydrated species are compared with reported for the monohydrate of tacrine, the RMSDs values decrease with both methods from 1.5 to 0.8 ppm. Note that the two methods predict practically the same ^1H NMR chemical shifts for the di-hydrated species. On the contrary, the ^{13}C NMR chemical shifts are predicted between 1.8 ppm for the anhydrous species and 19.6 ppm for the di-hydrated one with the B3LYP/6-311G* method while with the other method the RMSD value decreases to 13.3 ppm. These differences observed are attributed to 6-311G* basis set and to solvent used.

6. Electronic spectra

A comparison of experimental electronic spectrum of hydrochloride monohydrate tacrine in methanol solution with the predicted for the anhydrous and di-hydrated species in aqueous solution by using the B3LYP/6-311G* and wB97XD/6-311G* is shown in Fig. S4 [29]. Four bands with different intensities are observed in the experimental spectrum with a maximum located at 239 nm while the less intense at 216 and the other two at 322 and 335 nm. Only two bands at 475 and 650 nm shows the anhydrous species. The UV spectrum predicted for di-hydrated species with the B3LYP/6-311G* method presents an intense band at 611 nm while the wB97XD/6-311G* method predict two bands and a shoulder at 224, 281 and 349 nm, respectively. Hence, the anhydrous species is not present in an aqueous solution and the best UV spectrum of di-hydrated species is predicted with the wB97XD/6-311G* method. These absorption bands observed are related to the $\pi\rightarrow\pi^*$, $n\rightarrow\pi^*$ and $\pi^*\rightarrow\pi^*$ transitions predicted for both species by NBO calculations. As was previously mentioned, probably the freebase, cationic species of tacrine can exist in solution [1].

7. Conclusions

In this work, the theoretical structures of di-hydrated hydrochloride tacrine and its properties were determined in gas phase and aqueous solution. The results obtained by using B3LYP/6-311G* and wB97XD/6-311G* levels of theory were compared with the reported for the anhydrous species. The main results considering the effects of dispersion by using the wB97XD method are:

- Both methods evidence strong changes in the positions of two water molecules.
- Corrected and uncorrected energy values obtained with the wB97XD/6-311G* method in gas phase are similar to predicted with the B3LYP/6-31G* method.
- The dipole moment value for the di-hydrated species considering the dispersion (20.07 D) is similar to observed for the anhydrous species (20.42 D) while the V in gas phase (288.1 $Å^3$) is comparable to predicted in aqueous solution with the B3LYP/6-31G* method.

Table 7
Scaled internal force constants for di-hydrated and anhydrous hydrochloride tacrine in gas phase by using the B3LYP/6-311G* and wB97XD/6-311G* methods compared with other species with different properties.

Force constants	B3LYP/6-311G* method		
	Tacrine		
	B3LYP/6-311G*[a]	wB97XD/6-311G*[a]	B3LYP/6-311G*[b]
	Di-hydrated		Anhydrous
$f(\nu O\text{-}H)$	7.20	7.75	
$f(\nu NH_2)$	5.81	6.20	5.34
$f(\nu N\text{-}H)$	6.18	6.39	6.65
$f(\nu C\text{-}N)$	7.37	7.61	7.11
$f(\nu C\text{-}H)_{A1}$	5.15	5.19	5.12
$f(\nu C\text{-}C)_{A1}$	6.50	6.64	6.38
$f(\nu CH_2)$	4.73	4.79	4.72
$f(\delta CH_2)$	0.74	0.73	0.72
$f(\delta_{H2}O)$	0.67	0.69	

Other species

Force constants	B3LYP/6–311++G** method		B3LYP/6-31G* method	
	Hydrochloride		Hydrobromide	Di-hydrated
	Rimantadine[c]	Adamantadine[d]	Scopolamine[e]	Trehalose[f]
$f(\nu O\text{-}H)$			7.13	6.88
$f(\nu N\text{-}H)$	4.81	4.99	2.81	
$f(\nu C\text{-}N)$	3.81	4.78	3.72	
$f(\nu C\text{-}H)$	4.66	4.70	5.15	4.71
$f(\nu C\text{-}C)_R$	4.39	6.11	3.91	4.14
$f(\nu CH_2)$	4.65	4.71	4.84	4.81
$f(\delta CH_2)$	0.73	0.73	0.76	0.82
$f(\delta_{H2}O)$				0.70

Units are mdyn $Å^{-1}$ for stretching and mdyn Å rad^{-2} for angle deformations.
[a] This work.
[b] From Ref. [1].
[c] From Ref [28].
[d] From Ref [31].
[e] From Ref [26].
[f] From Ref [14].

- As expected, the di-hydrated species of tacrine present higher V and μ values than the anhydrous one due to the two water molecules.
- The solvation energies with both methods present practically the same values and higher than the anhydrous one.
- The atomic charges show important differences on H atoms belonging to NH_2 and NH groups common to both anhydrous and di-hydrated species.
- Changes in the bond orders of di-hydrated species are observed when the medium change from gas to water. Thus, in solution the di-hydrated species is more strongly linked to two water molecules and higher solvation energy value for this species is observed.
- The NBO studies suggest higher stability of di-hydrated species in solution due to its higher solvation energy while the AIM calculations support the lower stability of di-hydrated species in solution in agreement with its higher reactivity in this medium.
- Both anhydrous and di-hydrated species of tacrine evidence high reactivity but the wB97XD/6-311G* method predict higher gap values than the B3LYP/6-311G* one.
- Both methods predict different assignments and scaled force constants, presenting higher force constants values with the wB97XD/6-311G* method.
- Good concordances are observed from comparisons of predicted IR, Raman and ^1H NMR spectra with both methods with the experimental ones however, the ^{13}C NMR and UV spectra evidence better correlations with the wB97XD/6-311G* method.

Funding statement

This research did not receive any specific grant from funding agencies in the public, commercial, or not-for-profit sectors.

Data availability statement

Data will be made available on request.

Table 8
Observed and calculated ^{1}H chemical shifts (δ in ppm) for the di-hydrated and anhydrous hydrochloride tacrine in aqueous solutions by using different level of theory.

H atom	B3LYP/6-311G*[a]	wB97XD/6-311G*[a]	B3LYP/6-311G*[b]	Exp[c]	Exp[d]
	Di-hydrated[a]		Anhydrous[b]		
16-H	1.97	1.88			1.9
17-H	1.66	1.53	1.56	1.6	1.9
18-H	2.23	2.09	2.23	2.4	2.6
19-H	2.22	2.09	2.43	2.4	2.6
20-H	1.87	1.79	1.79	1.8	1.9
21-H	1.63	1.53	1.60	1.6	1.9
22-H	2.78	2.65	2.73	2.4	2.6
23-H	2.80	2.73	2.51	2.4	2.6
24-H	8.71	8.10	7.64	7.5	8.25
25-H	7.12	7.21	7.30	7.3	7.4
26-H	4.83	4.79	7.35	7.4	3.1
27-H	8.25	7.69	5.45	4.8	8.1
28-H	7.43	7.46	7.46	7.5	7.4
29-H	7.61	7.67	7.68	7.5	7.7
30-H	11.44	11.60	7.97	7.5	8.5
33-H	1.94	1.84			1.9
34-H	2.06	1.81			1.9
36-H	0.12	0.15			
37-H	3.30	3.34			3.1
RMSD[b]	**1.5**	**1.5**	**0.2**		
RMSD[c]	**0.8**	**0.8**			

[a]This work GIAO/B3LYP/6-311G* Ref. to TMS.
[b]From Ref [1].
[c,d]From Ref [29].

Table 9
Observed and calculated^{13}C chemical shifts (δ in ppm) for the di-hydrated and anhydrous hydrochloride tacrine in aqueous solutions by using different level of theory.

H atom	B3LYP/6-311G*[a]	wB97XD/6-311G*[a]	B3LYP/6-311G*	Exp[c]
	Di-hydrated		Anhydrous[b]	
3-C	42.05	34.24	23.7	22
4-C	41.50	34.04	25.7	24
5-C	41.34	33.83	23.1	22
6-C	130.57	121.67	114.2	112
7-C	48.42	41.16	31.1	30
8-C	174.99	170.59	156.1	154
9-C	176.38	172.16	157.8	158
10-C	136.59	128.61	117.9	115
11-C	159.55	153.57	140.6	138
12-C	147.44	141.09	125.3	124
13-C	138.58	133.26	121.8	120
14-C	146.59	141.00	129.7	128
15-C	154.83	150.27	137.7	138
RMSD[a]	**19.6**	**13.3**	**1.8**	

[a] This work GIAO/B3LYP/6-311G* Ref. to TMS.
[b] From Ref [1].
[c] From Ref [29].

CRediT authorship contribution statement

Tom Sundius: Conceptualization, Formal analysis, Investigation, Methodology. **Silvia Antonia Brandán:** Investigation, Validation, Writing – original draft, Writing – review & editing.

Declaration of competing interest

The authors declare the following financial interests/personal relationships which may be considered as potential competing interests:The authors declare the following conflict of interests: Silvia Antonia Brandán is part of the Editorial Board for Heliyon Chemistry.

Acknowledgements

This work was supported by Consejo de Investigaciones Universidad Nacional de Tucumán (CIUNT) Project No. 26/D714.

Appendix A. Supplementary data

Supplementary data to this article can be found online at https://doi.org/10.1016/j.heliyon.2023.e20936.

References

[1] T. Sundius, S.A. Brandán, Structural, harmonic force field and vibrational studies of cholinesterase inhibitor tacrine used for treatment of Alzheimer's disease, Heliyon 9 (2023), e17280, https://doi.org/10.1016/j.heliyon.2023.e17280.
[2] M. Moris, T. De Samber, J. Vrijdag, W. De Borggraeve, L. Van Meervelt, Crystal structure of the orthorhombic pseudopolymorph for tacrine hydrochloride, Jeroen Jacobs, Acta Crystallogr. (2016) 771–774, https://doi.org/10.1107/S2052520616011094. **B**72.
[3] M.R. Yadav, P.R. Murumkar, R. Barot, R. Yadav, K. Joshi, M. Chauhan, Role of computational modeling in drug discovery for Alzheimer's disease, in: S. Kar, J. Leszczynski (Eds.), Current Trends in Computational Modeling for Drug Discovery. Challenges and Advances in Computational Chemistry and Physics, vol. 35, Springer, Cham, 2023, https://doi.org/10.1007/978-3-031-33871-7-3.
[4] Ó.M. Bautista-Aguilera, L. Ismaili, I. Iriepa, D. Diez-Iriepa, F. Chabchoub, J. Marco-Contelles, M. Pérez, Tacrines as therapeutic agents for alzheimer's disease. V, Recent Developments 21 (1) (2021) 162–174, https://doi.org/10.1002/tcr.202000107.
[5] M.S. Kohnehshahri, G. Chehardoli, M. Bahiraei, T. Akbarzadeh, A. Ranjbar, A. Rastegari, Z. Najafi, Novel tacrine-based acetylcholinesterase inhibitors as potential agents for the treatment of Alzheimer's disease: quinolotacrine hybrids, Mol. Divers. 26 (1) (2022) 489–503, https://doi.org/10.1007/s11030-021-10307-2.
[6] S. Djafarou, I.A. Khodja, H. Boulebd, Computational design of new tacrine analogs: an in silico prediction of their cholinesterase inhibitory, antioxidant, and hepatotoxic activities, J. Biomol. Struct. Dyn. 41 (1) (2021) 1–15, https://doi.org/10.1080/07391102.2021.2004232.
[7] A.D. Becke, Density-functional exchange-energy approximation with correct asymptotic behavior, Phys. Rev. A38 (1988) 3098–3100.
[8] C. Lee, W. Yang, R.G. Parr, Development of the Colle-Salvetti correlation-energy formula into a functional of the electron density, Phys. Rev. B37 (1988) 785–789.
[9] M.A. Iramain, M.V. Castillo, L. Davies, M.E. Manzur, S.A. Brandán, Structural and SQMFF study of potent insecticide 4′,4′-DDT Combining the FT-IR and FT-Raman spectra with DFT calculations, J. Mol. Struct. 1199 (2020), 126964, https://doi.org/10.1016/j.molstruc.2019.126964.
[10] E. Romano, M.E. Manzur, M.A. Iramain, S.A. Brandán, Effect of long-range corrections on Intermolecular interactions and Vibrational assignments of Ethylene Oxide Dimer. A Combined DFT and SQFF Study, Eur. J. Theoret. Appl. Sci. 1 (5) (2023) 409–425. https://doi.org/10.59324/ejtas.2023.1(5).32.
[11] P. Pulay, G. Fogarasi, G. Pongor, J.E. Boggs, A. Vargha, Combination of theoretical ab initio and experimental information to obtain reliable harmonic force constants. Scaled quantum mechanical (QM) force fields for glyoxal, acrolein, butadiene, formaldehyde, and ethylene, J. Am. Chem. Soc. 105 (1983) 7073, https://doi.org/10.1021/ja00362a005.
[12] G. Rauhut, P. Pulay, Transferable scaling factors for density functional derived vibrational force fields, J. Phys. Chem. 99 (1995) 3093–3100, https://doi.org/10.1021/j100010a019.
[13] T. Sundius, Scaling of ab-initio force fields by MOLVIB, Vib. Spectrosc. 29 (2002) 89–95.
[14] M.J. Márquez, D. Romani, S.B. Díaz, S.A. Brandán, Structural and vibrational characterization of anhydrous and dihydrated species of trehalose based on the FTIR and FTRaman spectra and DFT calculations, J. King Saud Univ. 30 (2018) 229–249, https://doi.org/10.1016/j.jksus.2017.01.009.
[15] Gaussian 16, Revision C.01 M.J. Frisch, G.W. Trucks, H.B. Schlegel, G.E. Scuseria, J.B. Foresman, D.J. Fox, Gaussian, Inc., Wallingford CT, 2019.
[16] S. Miertus, E. Scrocco, J. Tomasi, Electrostatic interaction of a solute with a continuum, Chem. Phys. 55 (1981) 117–129.
[17] J. Tomasi, J. Persico, Molecular interactions in solution: an overview of methods based on continous distributions of the solvent, Chem. Rev. 94 (1994) 2027–2094.
[18] A.V. Marenich, C.J. Cramer, D.G. Truhlar, Universal solvation model based on solute electron density and a continuum model of the solvent defined by the bulk dielectric constant and atomic surface tensions, J. Phys. Chem. B113 (2009) 6378–6396.
[19] P. Ugliengo, MOLDRAW Program, University of Torino, Dipartimento Chimica IFM, Torino, Italy, 1998.
[20] E.D. Glendening, J.K. Badenhoop, A.D. Reed, J.E. Carpenter, F. Weinhold, NBO 3.1, Theoretical Chemistry Institute, University of Wisconsin, Madison, WI, 1996.
[21] R.F.W. Bader, Atoms in Molecules, A Quantum Theory, Oxford University Press, Oxford, 1990. ISBN: 0198558651.
[22] F. Biegler-Köning, J. Schönbohm, D. Bayles, AIM 2000; A program to analyze and visualize atoms in molecules, J. Comput. Chem. 22 (2001) 545.
[23] B.H. Besler, K.M. Merz Jr., P.A. Kollman, Atomic charges derived from semiempirical methods, J. Comput. Chem. 11 (1990) 431–439.
[24] A.B. Nielsen, A.J. Holder, Gauss View 6.0, User's Reference, GAUSSIAN Inc., Pittsburgh, PA, 2019.
[25] R.G. Pearson, Absolute electronegativity and hardness correlated with molecular orbital theory, Proc. Natl. Acad. Sci. U.S.A. 83 (1986) 8440–8441.
[26] R.A. Rudyk, M.A. Checa, C.A.N. Catalán, S.A. Brandán, Structural, FT-IR, FT-Raman and ECD studies on the FB, CA and hydrobromide species of scopolamine alkaloid, J. Mol. Struct. 1180 (2019) 603–617, https://doi.org/10.1016/j.molstruc.2018.12.040.
[27] M.E. Manzur, S.A. Brandán, S(-) and R(+) species derived from antihistaminic promethazine agent: structural and vibrational studies, Heliyon 5 (2019), e02322, https://doi.org/10.1016/j.heliyon.2019.e02322.
[28] M.A. Iramain, J. Ruiz Hidalgo, T. Sundius, S.A. Brandán, A combined study on structures and vibrational spectra of antiviral rimantadine using SQMFF and DFT calculations, Heliyon 8 (2022), e10102, https://doi.org/10.1016/j.heliyon.2022.e10102.
[29] Available from: Web page, https://spectrabase.com/spectrum.
[30] G. Keresztury, S. Holly, G. Besenyei, J. Varga, A.Y. Wang, J.R. Durig, Vibrational spectra of monothiocarbamates-II. IR and Raman spectra, vibrational assignment, conformational analysis and *ab initio* calculations of *S*-methyl-*N*,*N*-dimethylthiocarbamate, Spectrochim. Acta 49A (1993) 2007–2026.
[31] S.A. Brandán, Normal internal coordinates Force fields and vibrational study of Species Derived from Antiviral adamantadine, Int. J. Quant. Chem. 121 (2) (2021), e26425, https://doi.org/10.1002/qua.26425.
[32] D. Romani, I. Salas Tonello, S.A. Brandán, Influence of atomic bonds on the properties of the laxative drug sodium picosulphate, Heliyon 2 (2016), e00190, https://doi.org/10.1016/j.heliyon.2016.e00190.
[33] M. Vakili, E. Romano, V. Darugar, S.A. Brandán, Behaviors of antiviral oseltamivir in different media. DFT and SQMFF calculations, J. Mol. Model. 27 (2021) 237, https://doi.org/10.1007/s00894-021-04962-3.
[34] M. Sorrenti, L. Catenacci, G. Bruni, B. Luppi, F. Bigucci, G. Bettinetti, Solid-state characterization of tacrine hydrochloride, J. Pharmaceut. Biomed. Anal. 63 (7) (2012) 53–61, https://doi.org/10.1016/j.jpba.2011.12.023.